

# **Effect of Nose Cone Geometry on N-Class Rocket Flight Performance**

DEN318 Third Year Project - April 2023

By Alex Pinel Neparidze

Supervisor: Dr. Fariborz Motallebi

SCHOOL OF ENGINEERING AND MATERIALS SCIENCE

ENGINEERING / MATERIALS  
THIRD YEAR PROJECT  
DEN318

APRIL 2023

DECLARATION

This report entitled:

**Effect of Nose Cone Geometry on N-Class Rocket  
Flight Performance**

Was composed by me and is based on my own work. Where the work of the others has been used, it is fully acknowledged in the text and in captions to table illustrations. This report has not been submitted for any other qualification.

Name: Alex Pinel Neparidze

Signed 

Date 25/04/2023

# **Abstract**

Rocketry and aerodynamics go hand in hand, the performance of a rocket can be substantially increased if its components are designed and optimised in accordance with the desired flight path of the vehicle. As the most forward-facing component of the rocket, the nose cone is subjected to the highest aerodynamic loads of the entire vehicle and its shape must therefore be thoroughly considered so as to ensure it can travel smoothly through the air at a wide range of velocities.

This report is part of a larger collaborative project meant to study and design the aerodynamic components of QM Aurora's N-Class high-power rocket. This investigation will focus on finding the most suitable nose cone geometries according to existing theory and data. The chosen geometries will then be subjected to several Computational Fluid Dynamics simulations from which data can be extracted on their aerodynamic characteristics and performance. The findings extracted from the simulations will dictate the choice of nose cone geometry and proportions for QM Aurora's first high-power rocket.

# List of Contents

Abstract.....	3
List of Contents.....	4
List of Symbols .....	5
Introduction.....	6
Literature Review .....	7
Chosen Geometries .....	11
Setup.....	13
Result Validation.....	15
Wall Y+ Values .....	15
Wave Visualisation .....	15
Result Analysis .....	18
Flow Visualisation.....	18
Drag Force .....	19
Pressure Distribution .....	23
Conclusion .....	26
Acknowledgements.....	29
References .....	30
Appendix .....	33

# List of Symbols

<b>CFD</b>	Computational Fluid Dynamics
<b>VK</b>	Von Karman
<b>PS</b>	Power Series
<b>NACA</b>	National Advisory Committee for Aeronautics
<b>A</b>	Cross-sectional area
<b>D</b>	Drag force
<b>R</b>	Radius
<b>L</b>	Length
<b>M</b>	Mach number
<b><math>M_\infty</math></b>	Free-stream Mach number
<b>P</b>	Pressure
<b><math>P_\infty</math></b>	Free-stream Pressure
<b><math>P_0</math></b>	Stagnation Pressure
<b><math>P_g</math></b>	Gauge Pressure
<b><math>C_D</math></b>	Coefficient of Drag
<b><math>C_p</math></b>	Coefficient of Pressure
<b><math>\beta</math></b>	Shock-wave angle
<b><math>\delta</math></b>	Semi-vertex angle
<b><math>\gamma</math></b>	Heat capacity ratio
<b><math>\rho</math></b>	Density
<b><math>\rho_\infty</math></b>	Free-stream Density

# Introduction

As part of the QM Aurora Initiative student society, it is planned to build a rocket participate in the 2023 edition of the European Rocketry Challenge (EuRoC), this rocket must reach a peak altitude of 9000 metres using a commercially acquired solid rocket engine. Such a rocket is expected to reach velocities of Mach 1.8 and must be designed and constructed according to the highest engineering standards to ensure it retains its structural integrity while also providing the best possible performance.

Nose cones are the forward-facing component of a rocket, their cone-like shape is meant to reduce aerodynamic drag by redirecting the incoming airflow. In the field of high-power rocketry, they are also commonly used to house a payload and necessary equipment to recover the launch vehicle. Therefore, the shape of the nose cone must be defined in such a way that payload is maximized while reducing aerodynamic drag to a minimum. Of course, different rockets are expected to perform in different ways, and thus their design must be influenced by specific mission parameters. QM Aurora's first high-power N-class rocket is expected to reach an apogee of 9000m, the main powerhouse propelling this rocket will be the N-class N1560 solid rocket engine manufactured by Cesaroni Technologies, this engine has a total impulse of 16803Ns and is expected to accelerate the vehicle to speeds upwards of 560m/s in less than 11 seconds [1]. This means the vehicle will quickly transition between the subsonic, transonic, and supersonic regimes, this will subject the airframe to intense and rapidly evolving shocks and forces. Given its position at the top of the rocket, the aerodynamics of the nose cone are the most critical of the entire vehicle, and its design will greatly affect the overall flight performance of rocket.

The main goal of this report is to research and understand the types of nose cones that will suit the aims of the N-class rocket best, and to measure the aerodynamic performance and characteristics of these nose cones through the use of Computational Fluid Dynamics (CFD), not only will this ensure the rocket is aerodynamically optimised for its task, but it will also provide valuable data for later work and construction done by the QM Aurora engineering team.

# Literature Review

The study of nose cone aerodynamics has been of great interest throughout the last century, for any decrease in drag directly relates to an increase in performance. Going as far back as the introduction of the Congreve rockets back in 1808, a mix of conical, blunt, or spherical noses were placed atop these primitive rockets [2], and further developments in ballistics throughout the 19<sup>th</sup> century saw the introduction of the tangent ogive and secant ogive geometries, far superior to simple cones in aerodynamic terms and still used in bullets and small rockets to this day. As the second world war came to a close in 1945, modern rocketry and supersonic flight became a reality, ushering in a new era of research and developments in rocket aerodynamics.

As man-made objects began to break the sound barrier, there was a renewed need to understand the behaviour of bodies at high speeds, advancements in slender body theory by researchers like Ludwig Prandtl, Theodore von Karman, and Hsue-Shen Tsien resulted in mathematical models that allowed for increased optimisation of aerodynamic bodies. More importantly, researchers Wolfgang Haack and William Sears independently derived the Sears-Haack body, which in theory provides the lowest wave drag at supersonic speeds [3]. Given the limitations of computing power at the time, extensive wind-tunnel experimentation was conducted at NASA during the 1950s and 1960s comparing the performance of these newly derived geometries and providing vast amounts of data still used to this day. For such aerodynamic bodies, drag was identified to be composed out of 3 main components: pressure drag, skin-friction drag, and wave drag [4]. pressure drag is caused by the pressure difference between the front and the wake of the object, which can create a suction effect at the back of the body, skin-friction drag on the other hand is caused by the friction between the body and the fluid and is most significant at low speeds, wave drag appears at supersonic speeds with the formation of shock waves around the body and is the main contributor to drag forces acting on a body beyond Mach 1, wave drag can mainly be minimised by adjusting the fineness ratio and geometry of the nose shape [4].

Furthermore, nose geometry alone cannot be taken as the only factor affecting its aerodynamic properties, the fineness ratio of the nose (that is the relation between the length and diameter of the nose) has also been found to have a great impact on the performance of vehicles. Research conducted by NACA's Langley Aeronautical Laboratory in 1949 compared the performance of sounding rockets flying through high-subsonic, transonic, and supersonic speeds with parabolic nose shapes at fineness ratios of 12.5:1, 8.91:1, and 6.04:1, it found that once the vehicle reached supersonic speeds increasing the fineness ratio directly correlated to a decrease in drag [5]. Nevertheless, the paper acknowledges the potential effect of the rocket

fins on the results. Later experiments by the National Advisory Committee for Aeronautics in 1958 [6], compared a variety of shapes at various Mach numbers and fineness ratios, the Von Karman geometry (a variant of the previously mentioned Sears-Haack) was found to present lower wave drag coefficients when using a higher fineness ratio in its design. Nevertheless, this decrease was found to be almost negligible beyond ratios of 5:1. Altogether, there seems to be a consensus that while higher ratios provide better performance, values above 5 or 6 do not only yield minimal improvements but also unnecessarily reduce the payload capacity of rockets unless the length of the vehicle is increased.

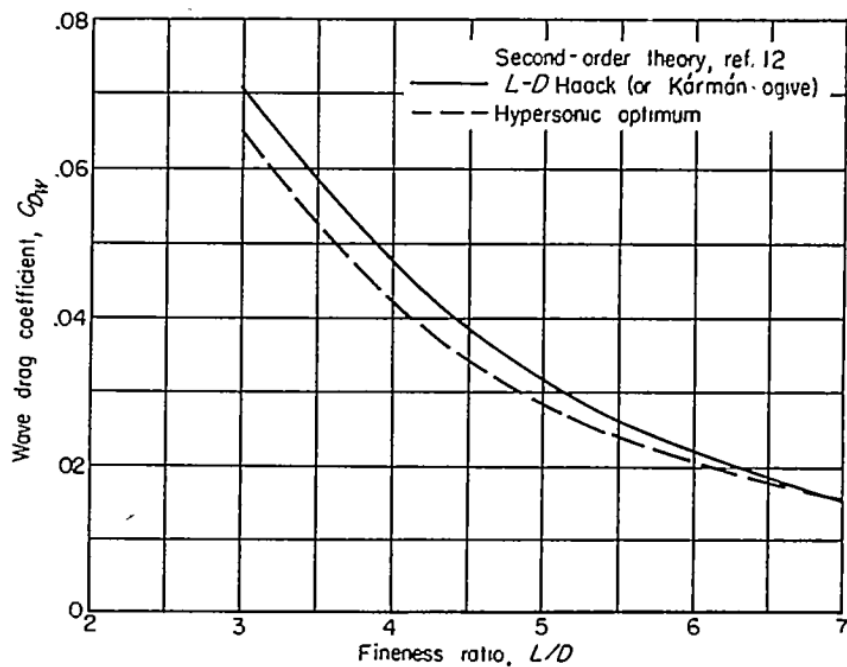


Figure 1 Variation of wave drag coefficient with fineness ratio [6]

Much interest has also been placed in the sharpness of nose cones; research conducted at Langley Research Center found that the coefficient of pressure at the tip of the nose would raise with increased nose bluntness [7]. More interestingly, NACA technical note 4201 compared a great variety of geometries of fineness ratio 3:1 at different Mach numbers, some highly blunted geometries presented the worst performance with ever increasing drag coefficients, however, some of the best performing shapes, such as the power series  $\frac{1}{2}$  also include a blunted tip [6]. This disparity indicates that while bluntness certainly has a considerable effect on the aerodynamic characteristics of a body, there are other factors at play that also play a significant role.

Decades of research and experimentation were instrumental in the definition of our modern understanding of high-speed aerodynamics, nowadays most of that information has been carefully processed and tabulated to allow for easier design of rockets and missiles. The *Design of Aerodynamically Stabilized Free Rockets Military Handbook* by the US Department of

Defence [4], the *AGARD Report 804* [8], and the DATCOM (Data Compendium) by the US Air Force [9] provide the most comprehensive overview of the component characteristics and performance that must be considered in rocket design. The general consensus among these reports is that ogive geometries provide the best performance at the subsonic regime, however at an almost negligible margin which is often offset by payload and size requirements. At transonic and supersonic speeds, the following visualisation obtained from Missile Configuration Design [10] attempts to illustrate the performance of certain nose shapes in the transonic and supersonic regimes:

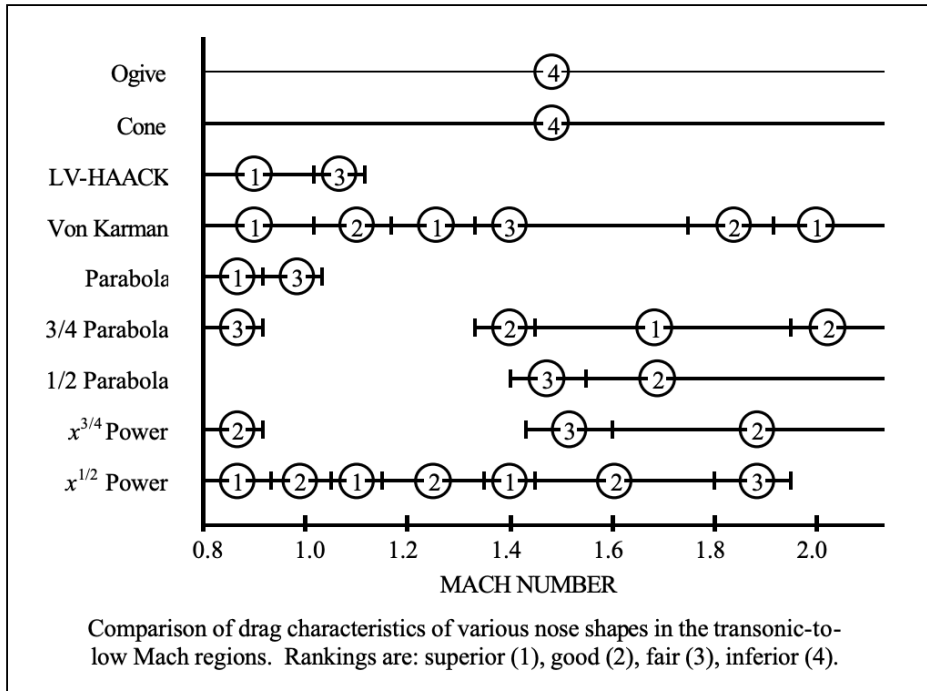


Figure 2 Comparison of drag characteristics for various nose shapes in the transonic to low Mach regions [10].

This particular chart was made using experimentally evaluated data mainly obtained from the USAF DATCOM and NACA Report 4201, with the gaps in the data corresponding to lack of research for that particular shape at the corresponding Mach numbers. According to this information, the classic conic and ogive shapes provide vastly inferior performance, and perhaps most strikingly the theoretically capable Haack body seems to yield decreasing results at low supersonic speeds. From this graph, it can easily be seen that Von Karman and Power Series  $x^{1/2}$  geometries offer the best performance within the Mach numbers Aurora's N-class rocket is expected to travel.

However, it must be noted that no single geometry can provide optimal performance throughout all flight regimes (subsonic, transonic, supersonic, and hypersonic), and how the choice of nose geometry depends more on the desired flight profile of the vehicle than the

aerodynamic characteristics of each shape. Furthermore, other factors such as payload capacity and the overall size of the vehicle have to be considered. For example, research conducted at the NASA Goddard Space Flight Center for the aerodynamic optimisation of the Nike Tomahawk sounding rocket found that an Ogive geometry with a fineness ratio of 3:1 proved optimal from the standpoint of stability, but when considering the bending moment and weight distribution of the payload inside the rocket, an increased ratio of 7:1 yielded an increase in apogee altitude of 6% [11].

Based on this information, it can be extracted from existing literature an theoretical knowledge that the Von Karman and Power Series X $\frac{1}{2}$  present the best performance for the desired range of velocities Aurora's rocket must face, additionally, it can also be observed that a fineness ratio value of 5:1 can reduce the aerodynamic drag on the vehicle while also ensuring payload volume capacity inside the rocket is not heavily reduced. Therefore, it is decided to carry on the investigation comparing the performance of the two selected geometries at a fineness ratio of 5:1.

## Chosen Geometries

Given that the main concern regarding Aurora's rocket is its efficiency when crossing the sound barrier and when travelling at supersonic speeds, mainly within the range of  $M=0.8$  and  $M=1.8$ , the Von Karman and the Power Series  $x^{1/2}$  seem to be the most suitable for the project when compared with all the other alternatives.

Theodore Von Karman, after whom this shape is named, developed an integral equation through which the wave drag of a slender body could be theoretically predicted. Using this equation, he derived a geometry which would present the least drag given a specific length and diameter (fineness ratio) [15]. Ever since, Von Karman's theoretical model has been used to derive other geometries optimised for different parameters such as internal volume. These mathematically optimised geometries now form part of what is known as the Haack series, which are formed using the following equations [12]:

$$y = \frac{R}{\sqrt{\pi}} \sqrt{\phi - \frac{1}{2} \sin(2\phi) + C \cdot \sin^3(\phi)} ; \quad \text{Eq.1}$$

$$\phi = \cos^{-1}\left(1 - \frac{2x}{L}\right)$$

Where the parameter  $C$  is chosen depending on the desired parameter optimisation, for Von Karman's geometry derived for fineness ratio, this value is taken as zero [12]. Solving Eq.1 for a model of fineness ratio of 5:1 (radius of 10mm and length of 100mm) yields the following shape:

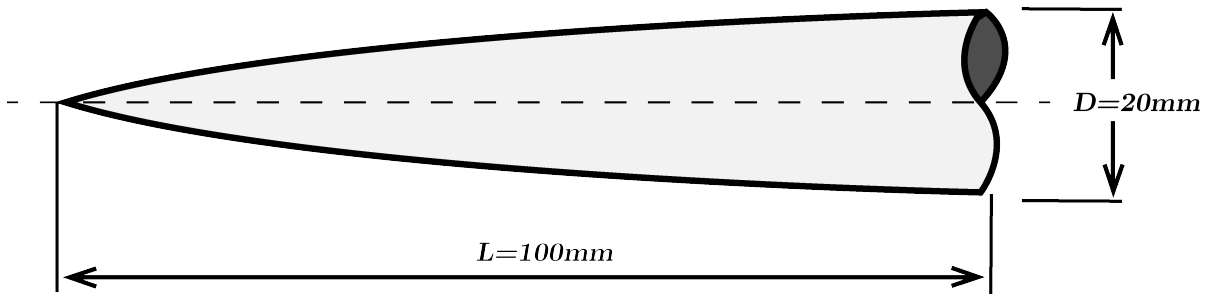


Figure 3 Von Karman nose cone at fineness ratio of 5:1

The power series on the other hand, is far simpler in nature, as it is obtained by rotating a parabola about its axis [12]. While the geometry is also obtained from the desired length and diameter of the nose, the derivation for this shape is far simpler than the previous mathematically optimised one, and is mainly defined by the fineness ratio and the value of the exponent  $n$  as can be seen in the following equation [6]:

$$y = R \left( \frac{X}{L} \right)^n \quad \text{Eq.2}$$

Different values of  $n$  are used to alter the bluntness of the nose cone, for the  $x^{1/2}$  variant of the Power Series this value is taken as 0.5 [6]. Computing Eq. 2 for the same model dimensions offers the following result:

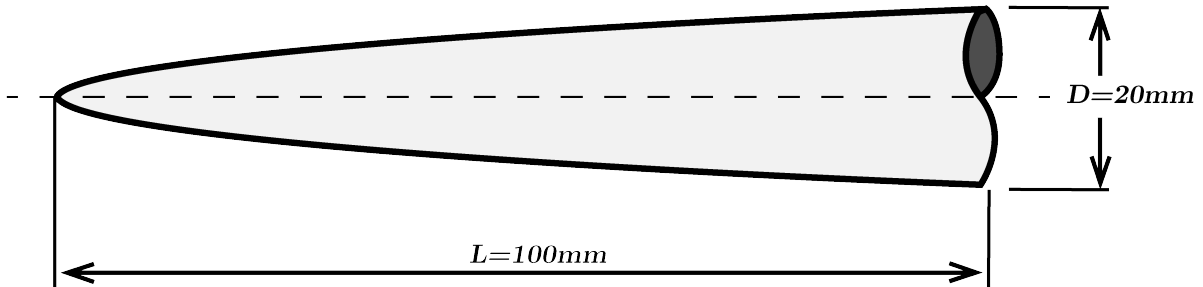


Figure 4 Power Series nose cone at fineness ratio of 5:1

The resemblance between the two geometries is rather striking, however, that might justify their better performance under the expected flight conditions, as similar shapes should naturally offer similar results. Superimposing the two shapes does reveal some of their differences:

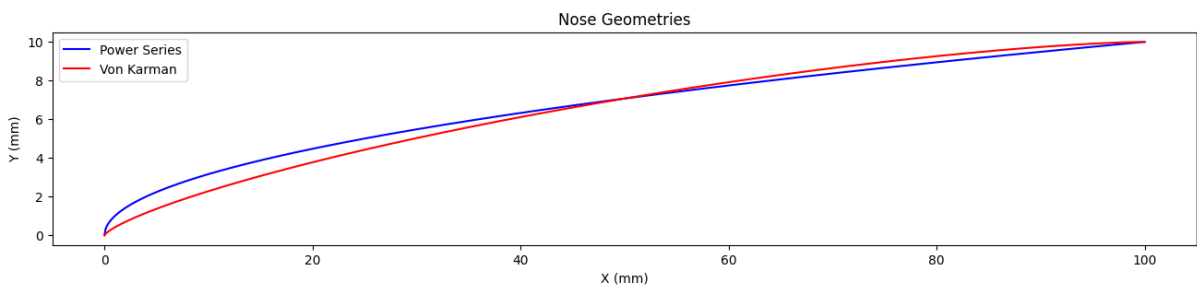


Figure 5 Comparison of the two nose geometries

At first glance, it can be easily noticed that the Power Series (blue) is blunter at the top than its counterpart (red), and while the overall silhouette is otherwise very similar, it must be noted that the transition from nose to body tube for Von Karman is smoother, this might have a significant effect beyond Mach 1 as the change in angle might result in the appearance of expansion waves at the point of transition [13].

# Setup

To compare the aerodynamic performance of the two selected nose cone geometries, Computational Fluid Dynamics (CFD) analysis is performed using the Siemens Star CCM+ software. Several simulations are to be conducted for both shapes under the same conditions and at increasing airflow Mach numbers, from these simulations data can then be extracted for drag force, pressure distribution, and airflow behaviour around the objects.

Two CAD models are made for each nose geometry using the shape equations previously mentioned, to predict the behaviour of the nose cones more accurately on a real rocket, a body tube section of 160mm is connected to the nose cones, this has the added benefit of eliminating the effects of base drag on the objects, which in a real rocket would affect the entire vehicle instead of the nose cone. Base drag is caused by the pressure difference between the front and wake of a body, which can result in a suction effect at the rear of the object, by neglecting this form of drag allows for more drag readings based entirely on the nose geometry and not the wake formation behind it [14]. The two geometries are compared using the same rectangular domain measuring 350mm in height and 380mm in length and width.

Given the number of simulations that must be performed, the meshing process is designed so as to produce the highest quality results without requiring vast processing power. A trimmed cell mesher is used to generate the mesh due to its high computational efficiency and performance in aerodynamic cases [16], this divides the domain into a grid of hexahedral cells which are programmed to become finer the closer they are to the nose cone profile. Additionally, a prism layer mesher is used to generate an inflation layer meant to represent the boundary layer on the surface of the bodies [17].

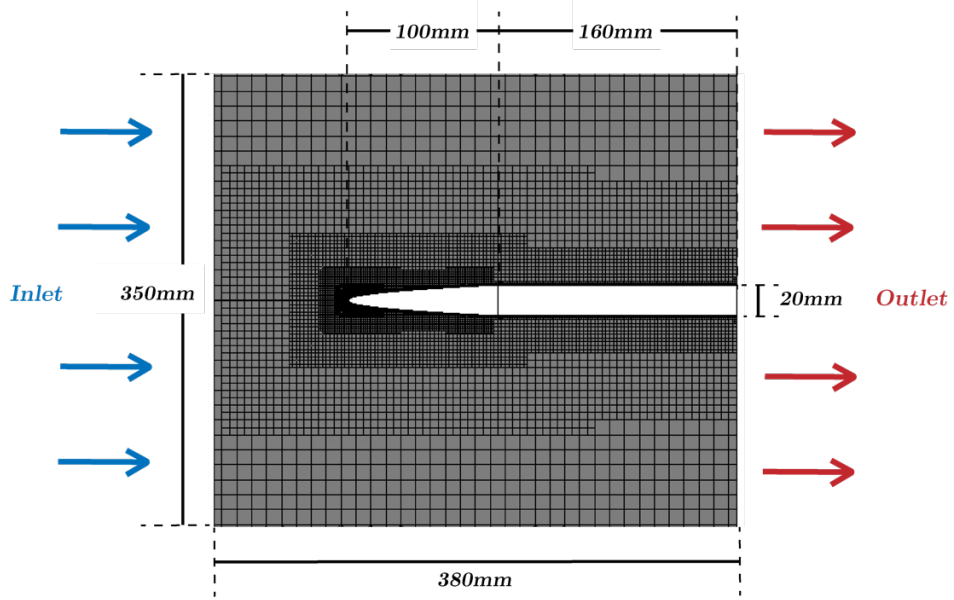
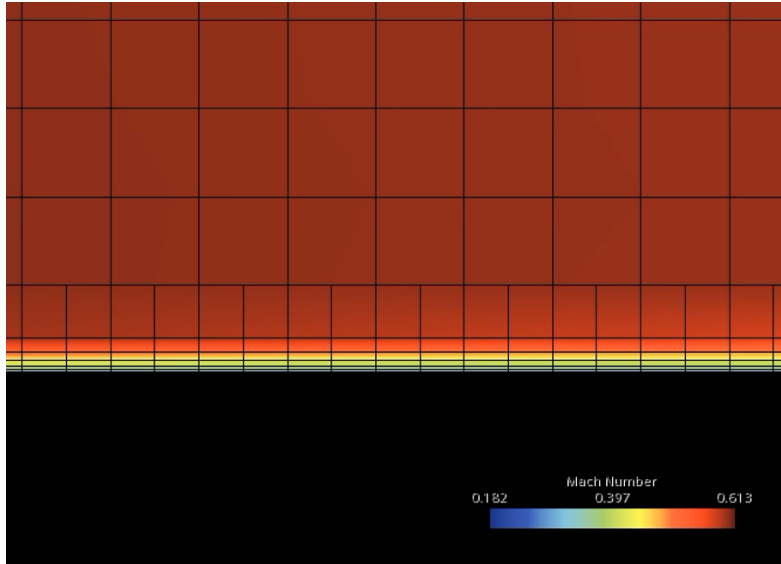


Figure 6 Domain mesh for the simulation setup



*Figure 7 Inflation layers at the wall of the body*

The physics settings of the model are chosen to accurately represent the flow conditions for Mach numbers ranging between 0.2 and 2. To account for the compressibility of the air, a real gas equilibrium air model is selected. The K-Epsilon turbulence Reynolds-Averaged Navier-Stokes model is chosen to simulate the viscous flow and turbulence around the object this model was chosen due to its good performance for supersonic flows and its simpler convergence compared to other models, which allows for various simulations to be run in a reasonable timeframe without requiring vast computational resources [18]. Furthermore, Coupled Energy and Coupled Flow models with 3<sup>rd</sup> order MUSCL discretization is selected due to its great capacity to handle the shocks and discontinuities that arise at supersonic speeds [19].

Finally, the boundary conditions must be specified, five such boundaries are defined for this simulation: velocity inlet, pressure outlet, chamber walls, nose cone, and body tube. A velocity inlet is used to generate an airflow of specified Mach number and with a free-stream pressure equivalent to atmospheric pressure at sea level (101325 Pa), the pressure outlet on the other hand is set with a gauge pressure of zero. The chamber walls encasing the domain are set as walls with a slip Shear Stress Condition, so as to simplify the computation process, the nose cone and body regions on the other hand are set as normal walls so as to accurately portray the airflow behaviour around them.

Using this setup, 10 simulations are to be performed for each nose cone for Mach numbers of 0.2, 0.4, 0.6, 0.8, 1.0, 1.2, 1.4, 1.6, 1.8, and 2.0, this range encompasses the entire velocity profile of Aurora's N-class rocket which travels through the subsonic, transonic, and supersonic regimes, thus offering valuable data that will be used for the final choice of nose shape.

# Result Validation

Before proceeding with the analysis of the obtained results, it is important to verify that the performed CFD simulations can accurately portray the expected flow behaviour. This can be done by analysing the wall  $Y+$  value of each simulation and by comparing the airflow and wave formation around each nose cone with existing theory.

## Wall $Y+$ Values

The wall  $Y+$  is a dimensionless parameter which is commonly used to assess the quality of the mesh resolution in a simulation. It is defined as the ratio of the distance of the first computational cell from the wall to the wall shear stress, multiplied by the molecular viscosity of the fluid [20]. For this particular set of simulations, a  $Y+$  value of 1 would indicate that the simulations provide accurate predictions of near-wall physics [26]. However, the general consensus seems to indicate that values of up to 30 are also considered to be accurate while requiring fewer computational resources.  $Y+$  values within the range of 2 to 5 were measured for subsonic simulations, once the speed of sound is crossed, values begin to increase with Mach number with a maximum of 28 measured for the Von Karman simulation at Mach 2.0. This seems to indicate that the mesh used is more suitable for subsonic speeds, and while all values are still within the desirable range, further mesh refinement would be suitable in future simulations to keep all results accurate.

## Wave Visualisation

The accuracy of the results at supersonic speeds can be measured by comparing the airflow and wave formation around each cone with existing theoretical models. Here, the flow analysis for both shapes is performed for the simulations at Mach 1.2.

For the Von Karman shape at a Mach number of 1.2, an oblique shock wave forms at the tip of the cone and expansion fans can be observed in the transition from the nose to the body. By measuring the angles of these waves and knowing the free-stream Mach number ( $M_\infty = \mathbf{1.2}$ ) and pressure ( $P_\infty = \mathbf{101325}$ ) it is possible to compare the results with the theoretical and empirical models presented in NACA Report 1135 [21]:

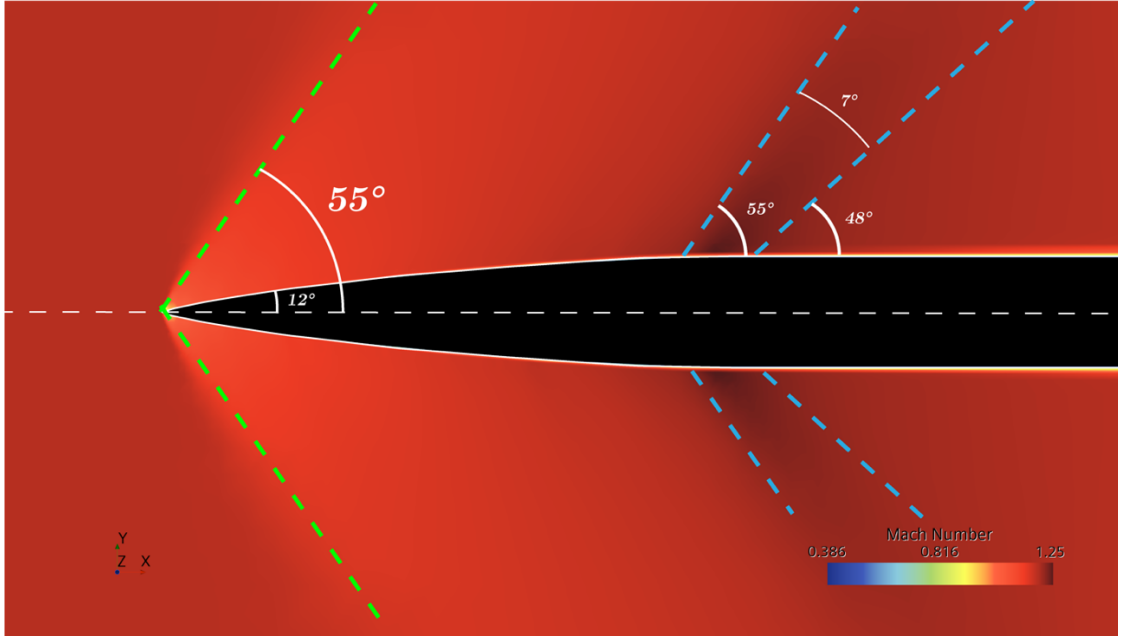


Figure 8 Wave formation for Von Karman at  $M=1.2$

NACA Report's chart 5 can be used to find the variation of cone semi-vertex angle  $\delta$  with shock-wave angle  $\beta$  for various free-stream Mach numbers. As can be seen in the previous figure, the angle  $\beta$  between the axis of the nose and the shockwave is of  $55^\circ$ , finding the semi-vertex angle  $\delta$  on the other hand requires that the Von Karman geometry be approximated as a cone [22], this can be done by taking the tangent of the geometry close to the tip which gives an angle  $\delta$  of  $12^\circ$ . Using the chart, it can be seen that for the measured two angles the free-stream Mach number must be of 1.2, which matches the free-stream velocity set for this simulation.

Furthermore, the Mach number immediately after crossing the shock wave  $M_2$  can also be calculated using the following equation [21]:

$$M_2 = \sqrt{\frac{(\gamma - 1)M_1^2 \sin^2(\beta) + 2}{(\gamma - 1) + 2M_1^2 \sin^2(\beta)}} / \sin^2(\beta - \delta) \quad \text{Eq.3}$$

$$M_2 = \sqrt{\frac{(1.4 - 1)1.2^2 \sin^2(55) + 2}{(1.4 - 1) + 2 * 1.2^2 \sin^2(55)}} / \sin^2(55 - 12) = 1.017$$

Such a reduction in Mach number matches the obtained results, where a clear change in colour from red to orange can be seen in figure 8 indicating a lower air speed over the nose cone.

This same validation method cannot be used for the equivalent Power Series simulation, as can be seen in the following figure the shock wave formation at the tip of the nose is detached [6], meaning that the same empirical data cannot be used.

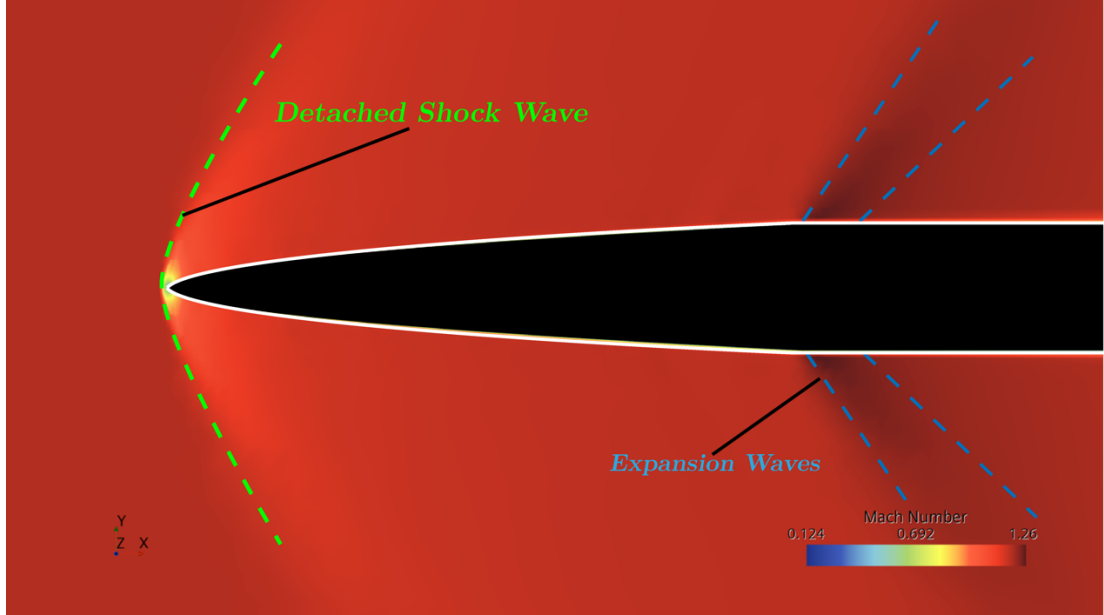


Figure 9 Wave formation for Power Series at  $M=1.2$

However, it is still possible to understand the accuracy of the simulation by measuring the stagnation pressure  $P_0$  at the tip of the cone. Unlike real world wind-tunnel testing where free-stream velocity and pressure are determined by a set value for the stagnation pressure, the opposite is true for CFD, meaning that the simulated stagnation pressure can be compared with theoretical values calculated through the isentropic process [23]:

$$\frac{P_0}{P_\infty} = \left(1 + \frac{\gamma - 1}{2} M_1^2\right)^{\frac{\gamma}{\gamma-1}} \quad \text{Eq.4}$$

$$P_0 = P_\infty \left(1 + \frac{\gamma - 1}{2} M_1^2\right)^{\frac{\gamma}{\gamma-1}} = 101325 \left(1 + \frac{0.4}{2} 1.2^2\right)^{3.5} = 245709 \text{ Pa}$$

Looking at the pressure distribution for this particular simulation in the appendix, it can be seen that the maximum gauge pressure over the nose cone is of 140627 Pa, this can be converted to absolute pressure by adding the free-stream pressure resulting in a simulated stagnation pressure of 241952 Pa, the percentage difference between the obtained and the calculated value is of 1.52%

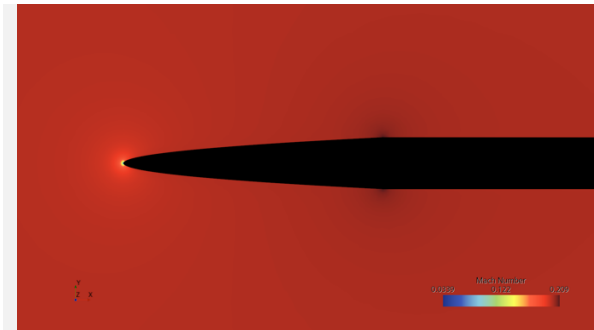
# Result Analysis

For each of the 20 simulations performed, data was collected on the airflow and wave formation, drag force acting on the nose cones, and pressure distribution around the profiles. Given the vast array of data, the complete results are presented in the appendix section of this report. This section will mainly focus on the results obtained at Mach numbers of 0.2, 1.2, and 1.8 so as to illustrate the behaviour of both shapes in all three flight regimes.

## Flow Visualisation

The following Mach contours illustrate the velocity of the air flowing around both nose cone geometries through the subsonic, transonic, and supersonic regimes:

Power Series



Von Karman

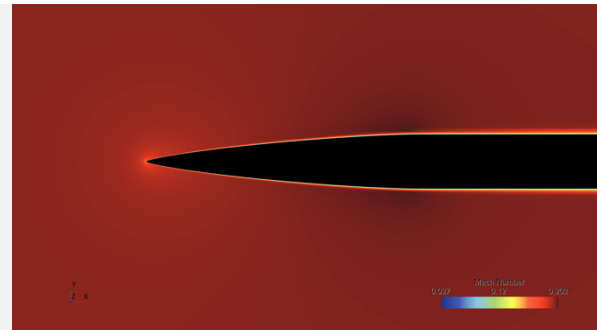


Figure 10 Flow at  $M=0.2$

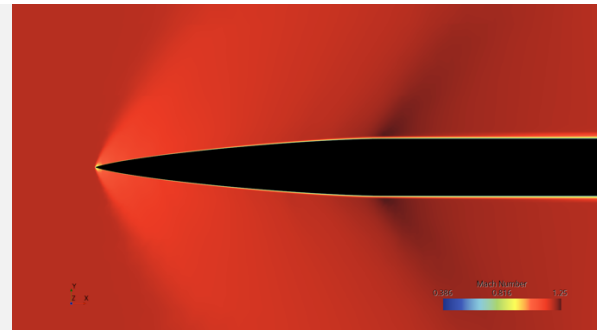
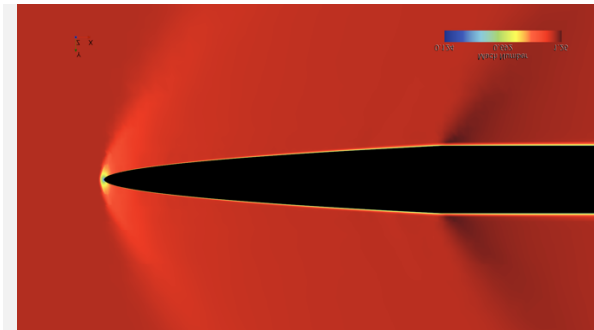


Figure 11 Flow at  $M=1.2$

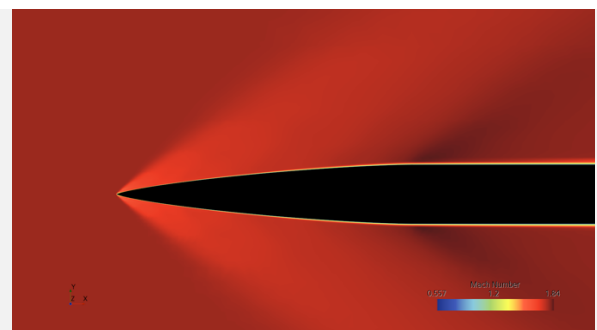
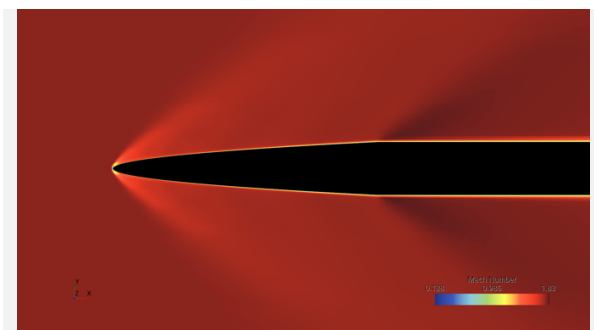


Figure 12 Flow at  $M=1.8$

At subsonic speeds the stagnation point is clearly identifiable at the tip of each nose, although it can be noted that the stagnation point for the Power Series seems to be larger than that of its counterpart, this can largely be attributed to the difference in bluntness of both shapes.

Breaking the sound barrier results in the formation of clearly visible shock waves at the bow of each nose. The shape of these shock waves appears to be different for each shape, the Von Karman presents a very sharp oblique wave that forms at the very tip of its profile, Power Series on the other hand results in the formation of a detached wave (also known as bow wave) which forms slightly ahead of the geometry and includes a clear curvature in its shape. Oblique shocks form when facing sharp edged obstacles while bow shocks appear from with spherical or blunted objects [13]. Expansion fans also form in both cases at the transition point between the nose and the body tube, this is because neither geometry presents a smooth and seamless transition between the two parts thus resulting in an acceleration of the airflow around the edge. As can be seen in figure 5 the Power Series presents a far rougher transition, this higher deflection angle is the reason why the expansion waves for this shape are more accentuated.

At higher Mach numbers, the shock waves become sharper with a clear decrease in the shock wave angle  $\beta$ . Interestingly, the detachment distance between the bow shock and the Power Series has also visibly decreased, this matches the experimental findings of [24].

Overall, the Mach number contour for both shapes is very similar, and any visible differences can be attributed to the difference in bluntness and nose-body transition smoothness of the two bodies.

## Drag Force

The drag forces acting on each nose cone were measured throughout each simulation. As previously mentioned, these measurements do not include the base drag caused due to the wake of the object, this is not only more accurate in the context of comparing shapes that are meant to fly in a rocket (the nose cone is not used as an independent projectile, it is attached to a vehicle) [6], but also allows for better comparison with the findings of previous reports. The resulting drag acting on each shape is presented below:

Table 1 Drag force at each Mach number

	M0.2	M0.4	M0.6	M0.8	M1.0	M1.2	M1.4	M1.6	M1.8	M2.0
<b>PS</b> <b>Drag (N)</b>	0.066	0.220	0.469	0.838	2.570	2.704	3.381	4.731	5.565	6.585
<b>VK</b> <b>Drag (N)</b>	0.064	0.225	0.468	0.814	2.673	2.609	3.217	4.827	5.376	5.900

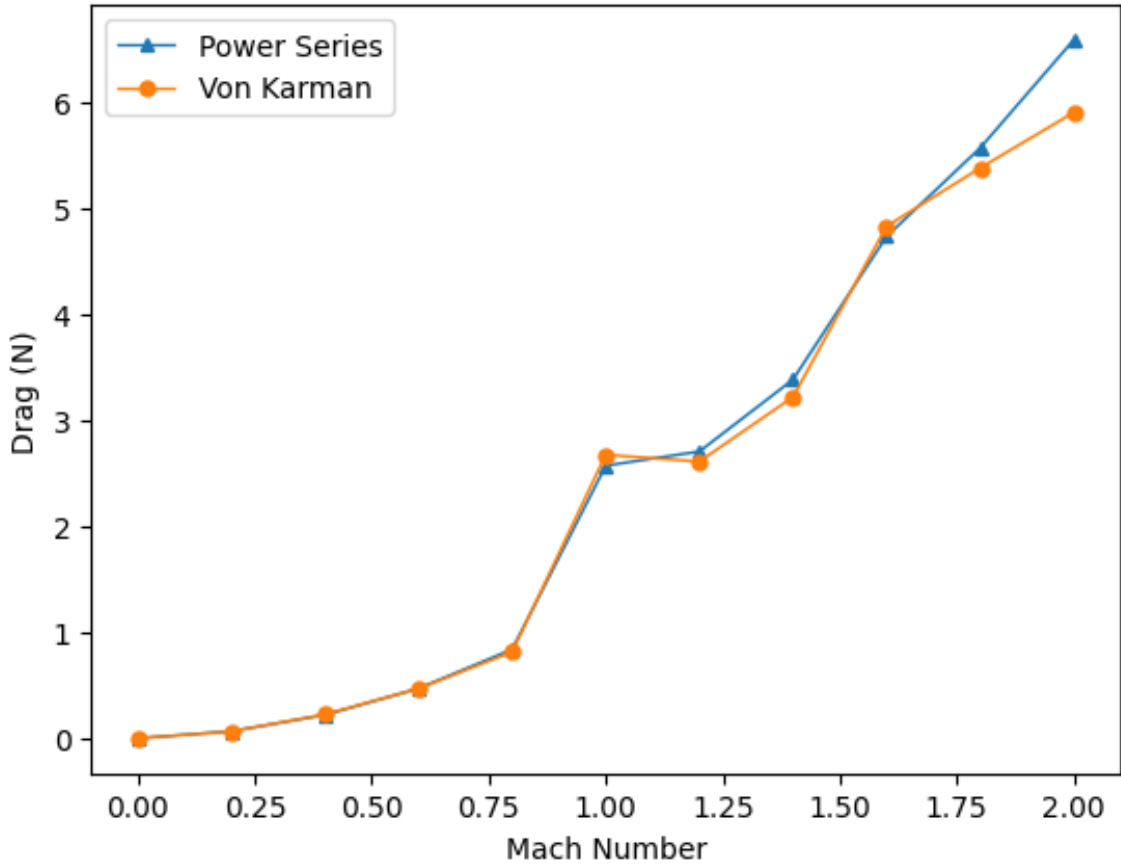


Figure 13 Drag vs Mach number

Here, it can clearly be seen how the drag forces steadily increase with airflow velocity. And for the first time, the performance of each geometry can be directly quantified and compared: at subsonic speeds the performance of the two shapes is nearly identical, this is in accordance with the existing literature which indicates that all nose cone geometries have similar behaviour in the subsonic regime [25], this can be attributed to the fact that drag at this velocities is mostly caused by skin friction and pressure, and given the very similar surface areas of the two shapes, any differences in pressure and skin friction drag can be taken as negligible [13].

Higher discrepancies appear when crossing the sonic speed threshold, Mach 1.0 is marked by a sharp increase in drag for the two profiles, with Power Series experiencing slightly milder drag forces. The onset of the aforementioned shock waves is now the main contributor to the drag experienced by the nose cones, wave drag is caused by the sudden increases in temperature and pressure induced by the shock waves [13]. As the Mach numbers keep climbing, so does the drag force for the Power Series, which more than doubles in strength between Mach 1 and 2. Von Karman on the other hand has more unpredictable behaviour, its drag force decreases in the transonic region between Mach 1 and 1.2 but then rapidly climbs surpassing the Power Series for a brief moment at Mach 1.6, but then provides increasingly better performance relative to its counterpart. This unexpected behaviour closely resembles the data in figure 2, where Power Series was ranked as superior in the transonic regime, and the performance of Von Karman was marked as inferior in the range between Mach 1.4 and 1.8 while also being classified as the best beyond Mach 1.8.

To better understand the drag forces acting on each shape it is possible to compute the coefficient of drag  $C_D$  using the following equation:

$$C_D = \frac{D}{\frac{1}{2} \gamma \cdot P_\infty \cdot M_\infty^2 \cdot A} \quad \text{Eq.5}$$

Where  $A$  is the cross-sectional area of the nose cone models ( $3.141*10^{-4}\text{m}^2$ ),  $P_\infty$  is the free-stream pressure of 101325 Pa,  $M_\infty$  is the corresponding free-stream Mach number,  $D$  is the drag force measured through CFD analysis, and  $\gamma$  is the specific heat ratio of air equals 1.4. Solving Eq.5 for each drag reading at their corresponding Mach number produces the following chart:

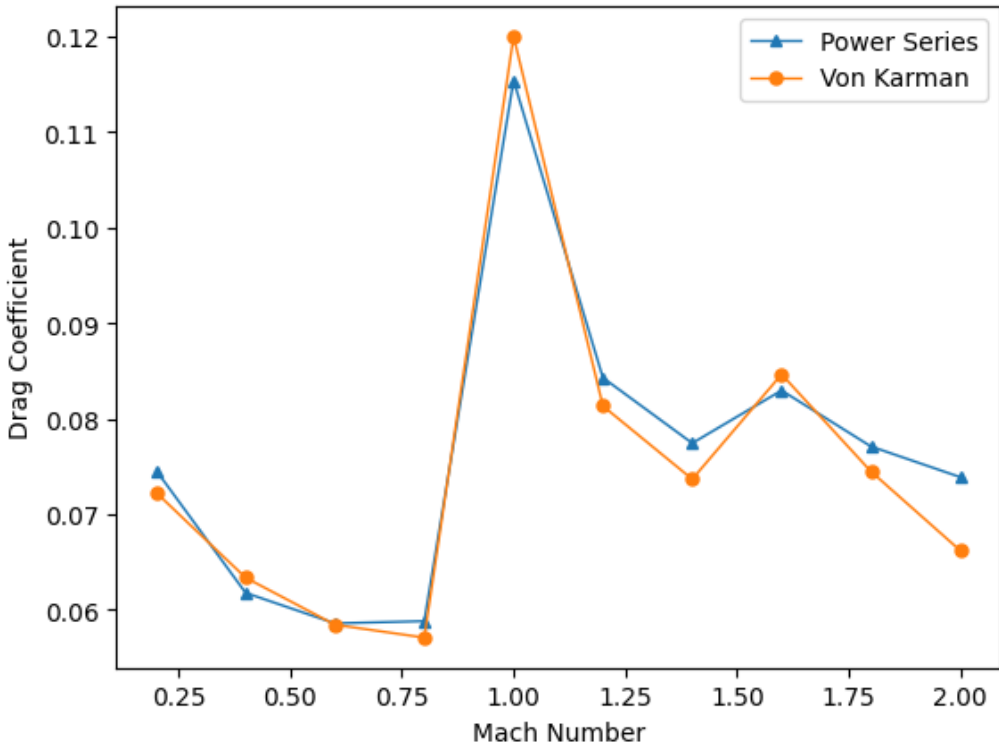


Figure 14 Drag coefficient vs Mach number.

This chart allows for a clearer visualisation of the drag characteristics for each geometry. Interestingly, the increase in drag force throughout the subsonic region translates into a decrease of drag coefficient for the same Mach numbers. The highest drag coefficient appears at Mach 1.0, with a sharp decline once the sound barrier is pierced. These results closely resemble the experimental findings of NACA report 4201 where drag coefficients for both shapes slightly increase in the supersonic region between Mach numbers 1.2 and 1.6 [6], to then decline again giving Von Karman a performance advantage at higher supersonic speeds. In his investigation, Taruansh Singh Qaumi [26] found overall very similar drag coefficients for Von Karman shapes of different fineness ratios within of Mach number values of 0.25 to 3.0, however, none of his results indicate the observed raise of drag coefficient at low supersonic speeds.

While it can clearly be seen that none of the two compared geometries holds a clear advantage throughout the entire flight profile, it is still possible to analyse which of the two has the overall best performance in terms of drag coefficient. This is done by calculating the average value for the drag coefficient of both shapes:

Table 2 Average drag coefficients

	Power Series	Von Karman	Percentage Difference
Average $C_D$	0.0765	0.0752	1.728%

Based on this information, Von Karman has a very slight advantage in performance of 1.728%, such a low value might seem negligible at first, but considering the extreme conditions the rocket must face throughout its flight, even the slightest improvement can have a great impact in the performance of the vehicle.

## Pressure Distribution

Lastly, the gauge pressure distribution along the profile of the two shapes was measured for each Mach number, and when paired with the previously discussed flow visualisation and drag analysis, it can offer great insight in the flow behaviour around the chosen nose cones. The following charts illustrate the measured gauge pressure for both shapes at Mach numbers of 0.2, 1.2, and 1.8:

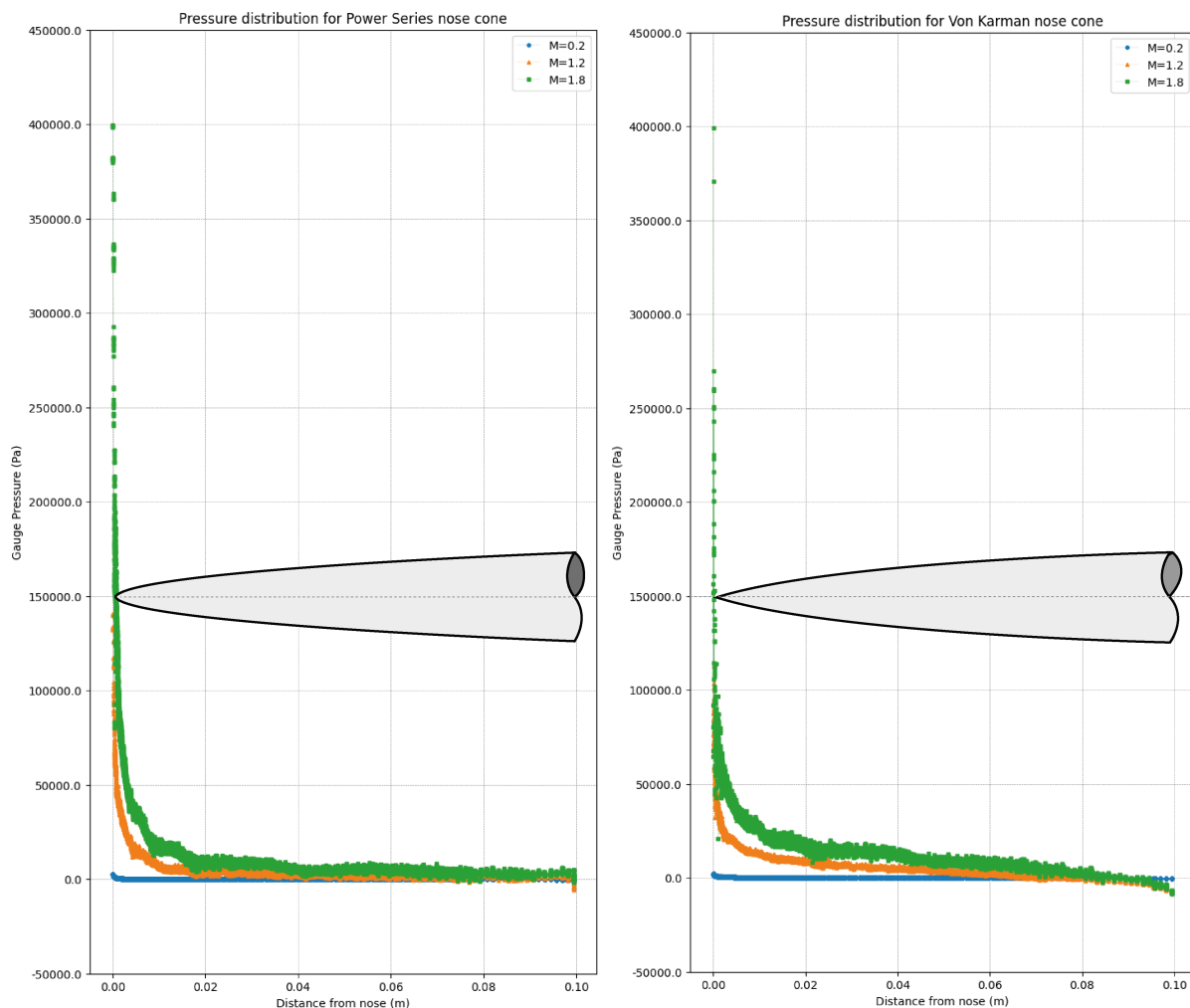


*Figure 15 Gauge pressure distribution*

Here, it can be observed how pressure is distributed along the surface of the Power Series and Von Karman nose cones. The fact that maximum pressures are the same for each shape at their corresponding Mach number is indicative of the fact that both simulations converged to

the same stagnation pressure and can therefore be compared. While both charts indicate a similar increase in pressure with Mach number, it can clearly be seen that due to the bluntness of the Power Series nose cone its tip is subjected to higher pressures, however, it must be noted that throughout most of its length Power Series has lower pressures than its counterpart. Furthermore, the Von Karman shape indicates a negative gauge pressure in its rear section, that means the pressure over that part of the surface (0.08-0.10m) has dropped below the free-stream pressure, the likely cause for this decrease in pressure is flow detachment over the profile as it transitions into the body tube [27].

Once again, a more accurate reading of the results can be obtained by calculating the pressure coefficients  $C_p$  over the nose cones, this is done by employing the following equation [21]:

$$C_p = \frac{p_g}{\frac{1}{2} \rho_\infty V_\infty^2} \quad \text{Eq.6}$$

Where  $p_g$  is the gauge pressure along the surface as portrayed in the previous charts,  $\rho_\infty$  is the free-stream air density ( $1.225 \text{ kg/m}^3$ ), and  $V_\infty$  is the free-stream airflow velocity. Solving Eq.6 for the same Mach numbers gives the following pressure coefficient profiles:

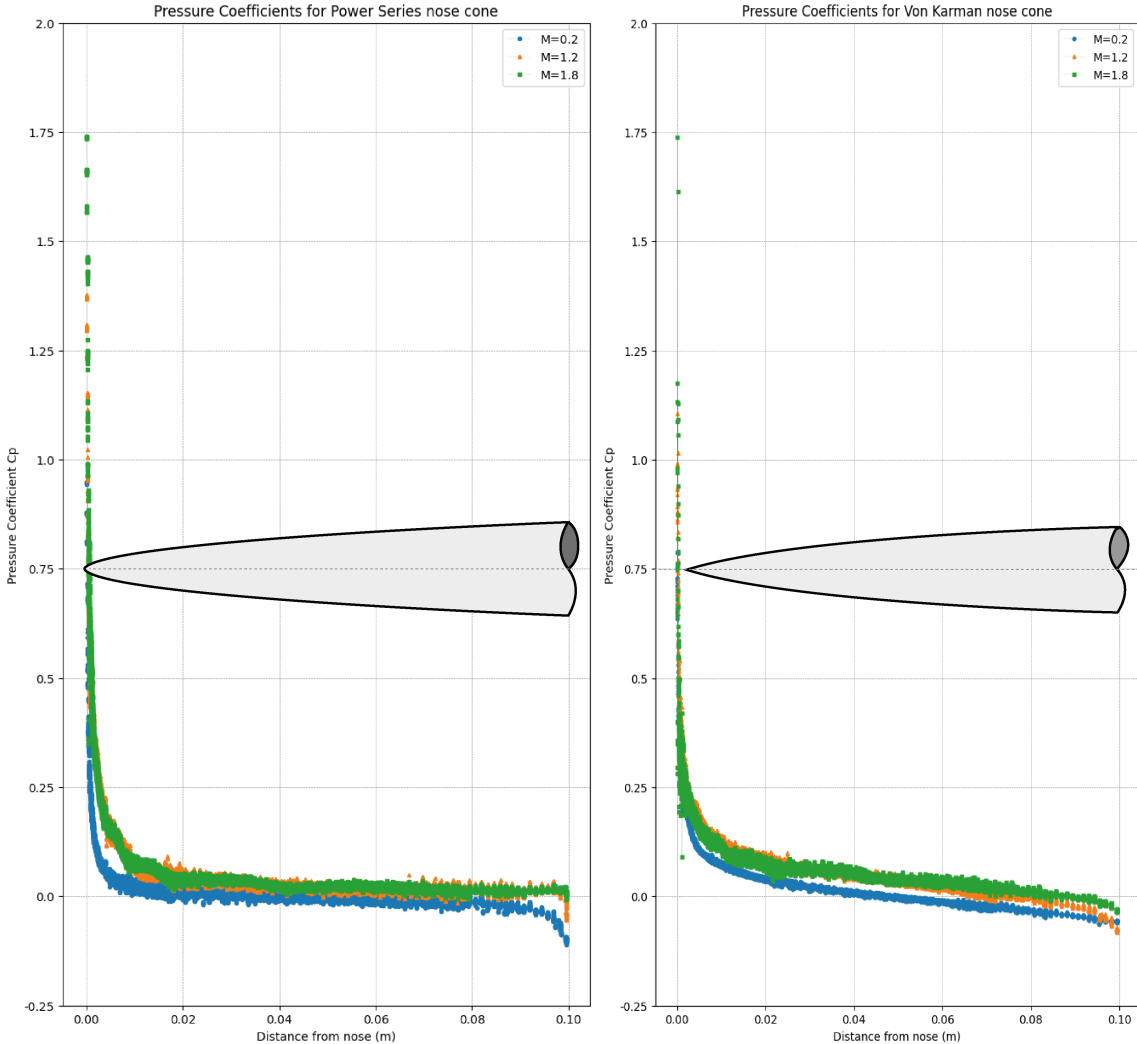


Figure 16 Pressure coefficient distribution

From this plot it can be observed that the lowest pressure coefficients are found at the lowest speed of  $M=0.2$ , and while  $M=1.8$  has the highest overall values for  $C_p$ , the frontal section range between 0.01-0.03m presents higher pressure coefficients at  $M=1.2$  for both geometries, this is likely caused by the effects of higher Mach number on the shock waves formed at the bow of the models [6]. Once more, it can be seen that the average  $C_p$  values between 0.02 and 0.08m are lower and remain constant for Power Series while Von Karman presents a more gradual decline in its values. This time it can also be appreciated how  $C_p$  becomes negative in the rear section of both shapes, thus corroborating the idea that this phenomenon is likely caused by the effects of the transition from nose to body tube.

# Conclusion

This project has been conducted with the goal of selecting the nose cone design for QM Aurora's rocket society N-class rocket capable of flying to altitudes of up to 9000m. Based on existing theory and previous experiments, it was found that two nose cone geometries: Power Series, and Von Karman would present the optimal aerodynamic performance for Aurora's rocket flight path. Furthermore, research conducted on a variety of nose shapes indicates that increasing the fineness ratio correlates to a decrease in drag, however, doing so beyond ratio values of 5:1 can prove inefficient in terms of payload volume and manufacturing. It was therefore decided to conduct a direct comparison using Computational Fluid Dynamics (CFD) of the aerodynamic characteristics of the two selected geometries at a fineness ratio of 5:1, the results would then dictate the final nose shape for Aurora's rocket while also providing updated computationally obtained data which could be compared with the experimental findings of reports conducting similar comparisons.

The quality of the CFD results was found to decrease at higher Mach numbers, however, the measured  $Y+$  values indicated that the quality of the data was still within engineering current practice regarding CFD analysis. Moreover, flow visualisation analysis was performed for both nose models at supersonic speeds, confirming that the shock wave patterns, and pressure distribution of the simulated setup successfully replicates the behaviour of supersonic flows, thus giving validity to the obtained results.

Expanding upon this flow visualisation, the air flow behaviour was compared for the three flight regimes the rocket must travel through (subsonic, transonic, and supersonic). Very similar patterns were observed for both geometries with the exception of a detached bow shock forming on the Power Series. It was also found that increasing the Mach number reduced the distance between the bow shock and the nose cone, matching the results observed in a report studying the effect of bluntness in symmetric nose shapes.

Measurements for drag suggest an almost indistinguishable performance between the two geometries at subsonic speeds, whereas noticeable discrepancies were visible after crossing the sound barrier, with Power Series presenting a slight advantage at transonic and low supersonic speeds and Von Karman displaying a clear advantage above  $M=1.6$ . This data was then used to calculate the drag coefficient at each Mach number, the calculated values mirrored the findings of previous experiments comparing the performance of different shapes at a fineness ratio of 3:1, nonetheless, a small inconsistency was found with a report comparing Von Karman nose cones at different fineness ratios, where there was no visible increase in drag coefficient between Mach 1.2 and 1.6. By taking the average drag coefficient value for each nose cone, it

was found that Von Karman is 1.728% more effective at mitigating drag than its blunter counterpart.

Lastly, the pressure distribution was compared along the length of both profiles, if each shape is divided into ‘tip’, ‘core’, and ‘rear’ sections, it can be observed that Power Series faces a greater total pressure at the tip while having a lower core pressure than the Von Karman equivalent. It is of special interest that both geometries show a decrease to negative pressure coefficient values in the rear section, this behaviour is attributed to the formation of expansion fans at the transition between nose and body tube, resulting in areas with reduced pressure and increased airflow Mach number.

For future investigations, performing an equivalent comparison using high-speed wind-tunnel testing would provide invaluable data to a field which has not seen extensive experimental research of this kind in decades. Such an experiment was the original plan for this project, but regrettably it was not possible to manufacture suitable metallic models of the two nose cones in time. Otherwise, for further computational analysis it would be recommended to increase the mesh refinement and perform more simulations for the same range of Mach numbers, this would allow for greater detail and quality in the final results.

Overall, based on the findings of this report it can be determined that a Von Karman nosecone with a fineness ratio of 5:1 is most suitable for Aurora’s N-Class rocket and will therefore be used in the construction of the launch vehicle.



*Figure 17 Acquired Von Karman nose (left) next to QM Aurora's Lil' Mary H-Class rocket.*

## Acknowledgements

I would like to offer my sincerest appreciation to my supervisor Dr. Fariborz Motallebi for the passion and interest with which he has guided me and my fellow classmates throughout this project. His continuous counselling both as a supervisor and as a lecturer have had a profound impact in me and have allowed me to see first-hand what it means to be a passionate aerospace engineer.

My special thanks also go to the marvellous team at the QM Aurora rocket society, who are working tirelessly to make our rocket a reality.

## References

1. Coker , J. (1998) Thrustcurve Hobby Rocket Motor Data, • ThrustCurve. Available at: <https://www.thrustcurve.org/motors/Cesaroni/16803N1560-P/> (Accessed: November 2, 2022).
2. Spearman, M.L., 1989, January. Historical review of missile aerodynamic developments. In Nielsen Engineering and Research, Inc., Missile Aerodynamics: NEAR Conference on Missile Aerodynamics.
3. Jones, R.T., 1956. Theory of wing-body drag at supersonic speeds (No. NACA-TR-1284).
4. Handbook, M., 1990. Design of aerodynamically stabilized free rockets. US Army Missile Command.
5. Hart, R.G. and Katz, E.R., 1949. Flight Investigations at High-Subsonic, Transonic, and Supersonic Speeds To Determine Zero-Lift Drag of Fin-Stabilized Bodies of Revolution Having Fineness Ratios of 12.5, 8.91, and 6.04 and Varying Positions of Maximum Diameter (No. NACA-RM-L9I30).
6. Perkins, E.W., Jorgensen, L.H. and Sommer, S.C., 1958. Investigation of the drag of various axially symmetric nose shapes of fineness ratio 3 for Mach numbers from 1.24 to 7.4 (No. NACA-TR-1386).
7. Nowak, R.J., Albertson, C.W. and Hunt, L.R., 1984. Aerothermal tests of a 12.5 percent cone at Mach 6.7 for various Reynolds numbers, angles of attack and nose shapes (No. L-15729).
8. NATO, A.G.A.R.D. (1996) Special Course on Missile Aerodynamics. Essex: Specialised Printing Services Limited.
9. Rosema, C. and Doyle, J. (2014). MISSILE DATA COMPENDIUM (DATCOM). WRIGHT-PATTERSON AIR FORCE BASE, OH 45433-7541: Aerospace Vehicles Technical Assessment and Simulation Branch Power and Control Division.
10. Chinn, S.S. (1961) Missile Configuration Design, McGraw-Hill Book Co., Inc., New York.
11. Hutton Jr, C.I., Mayo, E.E. and Weisskopf, G.A., 1965. Nike Tomahawk nose optimization studies (No. NASA-TM-X-55348).
12. A., G. and Sr., C. (1996). THE DESCRIPTIVE GEOMETRY OF NOSE CONES.

13. Anderson, J., 2011. EBOOK: Fundamentals of Aerodynamics (SI units). McGraw hill.
14. Sedney, R., 1966. Review of base drag. ARMY BALLISTIC RESEARCH LAB ABERDEEN PROVING GROUND MD.
15. Jamal, H., Naveed, S.M.F., Javed, M.Z., Ahsan, M. and Salamat, S., 2021. Optimal Wave Drag Reduction Technique for Fighter Aircraft Using von Kármán Ogive and Haack Series. *Pakistan Journal of Engineering and Technology*, 4(1), pp.151-158.
16. SIEMENS (2021) The third part of a series of introductory articles on Simcenter STAR-CCM+ simulation, focusing on meshing as the last step in geometry preparation., Siemens DISW. Available at: <https://community.sw.siemens.com/s/article/A-new-user-s-guide-to-STAR-CCM-simulation-Part-3-5-Meshing> (Accessed: March 15, 2023).
17. Patrik Růžička; Modeling of boundary layer and the influence on heat transfer with help of CFD. *AIP Conference Proceedings* 28 November 2018; 2047 (1): 020021. <https://doi.org/10.1063/1.5081654>
18. Bulat, M.P. and Bulat, P.V., 2013. Comparison of turbulence models in the calculation of supersonic separated flows. *World Applied Sciences Journal*, 27(10), pp.1263-1266.
19. van Leer, B. and Nishikawa, H., 2021. Towards the ultimate understanding of MUSCL: Pitfalls in achieving third-order accuracy. *Journal of Computational Physics*, 446, p.110640.
20. Versteeg, H.K. and Malalasekera, W. (2010) An introduction to computational fluid dynamics: The Finite Volume Method. Harlow: Pearson/Prentice Hall.
21. Staff, A.M.E.S., 1953. NACA report (1135) Equations, Tables and Charts for Compressible flow. Technical Report 1135. National Advisory Committee for Aeronautics.
22. Nielsen, J., 1988. Missile aerodynamics. American Institute of Aeronautics and Astronautics, Inc..

23. Motallebi, F. (2023). High Speed Aerodynamics (DEN6405) Advanced High Speed Aerodynamics (DENM405) Lecture Notes 1.
24. Czarnecki, K.R., 1961. Effects of Cone Angle, Mach Number, and Nose Blunting on Transition at Supersonic Speeds (Vol. 634). National Aeronautics and Space Administration.
25. Carvalho, L. and Claudino, G., 2019, October. CFD analysis of drag force for different nose cone design. In presented at the IX Forum de Pesquisa e Inovacao do Centro de Lancamento da Barreira do Inferno.
26. Qaumi, Taruansh Singh (2021): Aerodynamic Optimization of the Von Karman Nose Cone for a Supersonic Sounding Rocket. Toronto Metropolitan University. Thesis. <https://doi.org/10.32920/ryerson.14635638.v1>
27. Schaefer, J.W. and Ferguson, H., 1962. Investigation of separation and associated heat transfer and pressure distribution on cone-cylinder-flare configurations at Mach five. ARS Journal, 32(5), pp.762-770.

# Appendix

